JBC Papers in Press. Published on January 17, 2013 as Manuscript M112.419101
The latest version is at http://www.jbc.org/cgi/doi/10.1074/jbc.M112.419101

Thioredoxin-interacting protein mediates high glucose-induced reactive oxygen species (ROS) generation by mitochondria and the NADPH oxidase, Nox4, in mesangial cells.

Anu Shah[1,2,3,4], Ling Xia[2,4], Howard Goldberg[2,4], Ken W Lee[1,2,3,4], Susan E. Quaggin[1,3,4,] Ivan G. Fantus[1,2,3,4]

[1]Department of Medicine and Samuel Lunenfeld Research Institute, Mount Sinai Hospital, [2]Toronto General Research Institute, University Health Network, [3]Department of Physiology and [4]Banting and Best Diabetes Centre, University of Toronto, Toronto, ON, Canada.

To whom correspondence should be addressed: I. G Fantus, Mount Sinai Hospital, 60 Murray Street, Joseph and Wolfe Lebovic Building, Suite 5-028, Toronto, ON, Canada, M5T 3L9 Email: gfantus@mtsinai.on.ca Phone: 416-586-8665 Fax: 416-361-2657

Word Count: Summary (247 words); Manuscript (5173 words), Running Title (56 characters with spaces), Figures: 9

Running Title: *TxNIP is required for ROS generation and Nox4 expression*

CAPSULE

Background: Thioredoxin-interacting proteín (TxNIP) is upregulated by high glucose (HG), inhibits the antioxidant, thioredoxin and thereby implicated in oxidative stress.

Results: TxNIP deficiency protects mesangial cells from HG-induced oxidative stress and increased collagen by blocking mitochondrial glucose metabolism, NADPH oxidase and Nox4.

Conclusion: TxNIP controls ROS generation by regulating TCA cycle versus glycolytic glucose flux.

Significance: Inhibition of TxNIP is a promising approach to treat glucose toxicity

SUMMARY

Objective: Thioredoxin-interacting protein (TxNIP) is upregulated by high glucose and is associated with oxidative stress. It has been implicated in hyperglycemia-induced β-cell dysfunction and apoptosis. As high glucose and oxidative stress mediate diabetic nephropathy (DN), the contribution of TxNIP was investigated in renal mesangial cell reactive oxygen species (ROS) generation and collagen synthesis.

Research Design and Methods: To determine the role of TxNIP, mouse mesangial cells (MC) cultured from wild-type C3H and TxNIP-deficient Hcb-19 mice were incubated in HG. Confocal microscopy was used to measure total and mitochondrial ROS production (DCF and MitoSOX) and collagen IV. Trx and NADPH oxidase activities were assayed and NADPH oxidase isoforms, Nox2 and Nox4, and antioxidant enzymes determined by immunoblotting

Results: C3H MC exposed to HG elicited a significant increase in cellular and mitochondrial ROS as well as Nox4 protein expression and NADPH oxidase activation, while Hcb-19 MC showed no response. Trx activity was attenuated by HG only in C3H MC. These defects in Hcb-19 MC were not due to increased antioxidant enzymes or scavenging of ROS, but associated with decreased ROS generation. Adenovirus mediated overexpression of TxNIP in Hcb-19 MC and TxNIP knockdown with siRNA in C3H confirmed the specific role of TxNIP. Collagen IV accumulation in HG was markedly reduced in Hcb-19 cells.

Conclusions: TXNIP is a critical component of the HG-ROS signaling pathway, required for the induction of mitochondrial and total cell ROS and the NADPH oxidase isoform, Nox4. TXNIP is a potential target to prevent DN.

INTRODUCTION

Diabetic nephropathy (DN), a microvascular complication of diabetes mellitus, is a major cause of morbidity and mortality resulting in end stage renal disease requiring dialysis and/or transplantation (1-3). While chronic exposure to elevated levels of glucose is the central cause, the molecular pathogenesis remains to be completely defined (4). The pathological hallmarks of DN include increased mesangial matrix expansion associated with increased production and decreased degradation of extracellular matrix (ECM) proteins such as fibronectin, laminin and collagen (2, 5-8).

A major link between high glucose and cellular dysfunction is oxidative stress (9-10). Thus, it has been proposed that increased metabolic flux of glucose via mitochondrial glucose oxidation leads to the increased production of reactive oxygen species (ROS), such as $O_2^{\cdot-}$(superoxide), a byproduct of electron transport (9). ROS generation in excess of endogenous antioxidant neutralizing capacity leads to oxidative stress. This in turn leads to an inhibition of glyceraldehyde -3- phosphate dehydrogenase (GAPDH) activity, promoting increased flux through upstream glycolytic branch pathways, including the aldose reductase/polyol pathway, formation of reactive sugars and advanced glycation endproducts (AGEs), de novo synthesis of diacylglycerol (DAG) and chronic activation of PKCs and increased intracellular O-glycosylation via the hexosamine biosynthetic pathway (HBP) (9, 10). At the same time, ROS have been shown to be increased in the presence of high glucose by activation of NADPH oxidases (11-16). *In vivo* studies of diabetic rodents demonstrate protection against complications by antioxidants, by inhibition of NADPH oxidase and by genetic overexpression of antioxidant enzymes such as Cu, Zn

Superoxide Dismutase (SOD) (17-19). More recently, *in vivo* and *in vitro* evidence for upregulation by high glucose of NADPH oxidase subunits, e.g. $p22^{phox}$ and $p47^{phox}$, as well as the predominant renal isoform, Nox4, strongly support this concept (13-16, 20).

The importance of oxidative stress as a mediator of high glucose-induced pathology has led to studies of its regulation. One protein found to be markedly upregulated by high glucose in a number of cells, including mesangial cells and pancreatic β-cells is thioredoxin-interacting protein (TxNIP), also known as vitamin D upregulated protein one (VDUP1) (7, 21-24). TxNIP has been implicated in promoting oxidative stress by binding and inhibiting thioredoxins (Trx) 1 and 2, ubiquitous antioxidant oxidase-reductase enzymes localized to the cytosol and mitochondria respectively (21,25-27). Thus, by impairing ROS scavenging in high glucose TxNIP may contribute to "glucose toxicity". This has been observed in pancreatic β-cells as we and others have reported that TxNIP-deficient mice are relatively protected from the development of β-cell failure and diabetes induced by streptozotocin (28-30) and in the presence of insulin resistance (31). A similar role in promoting oxidative stress would implicate TxNIP in the pathogenesis of DN. To investigate this possibility and explore TxNIP action directly in the kidney, primary mesangial cells were cultured from wild-type control (C3H) and TxNIP-deficient (Hcb-19) mice and exposed to high glucose. TxNIP-deficiency protected the MC from high glucose induced increased ROS and collagen accumulation. Surprisingly, the lack of TxNIP was associated with a marked decrease in NADPH oxidase activity, ROS generation and Nox4 induction rather than a decrease in ROS scavenging. Furthermore, mitochondrial O^{2-} was not increased by high glucose in Hcb-19 cells while lactate production was augmented. These data place TxNIP upstream of NADPH oxidase activation by high glucose and suggest a potential Trx-independent action of TxNIP to promote mitochondrial metabolic flux, oxidative stress and DN.

RESEARCH DESIGN AND METHODS

Cell Culture

Mouse mesangial cells (MC, passages 5-12) from C3H (wild-type TxNIP) and Hcb-19 (TxNIP- deficient) mice (kindly provided by R. Davis, University of CA) were isolated and characterized as described (32, 33). They were propagated in Dulbecco's Modified Eagle's Medium (DMEM) supplemented with 10% FBS and 1% penicillin-streptomycin. At 70-80% confluence, cells were growth arrested with 0.5% FBS for 48h and incubated with either 5.6 mM (NG, normal glucose) or 25 mM (HG, high glucose) for the times indicated. Cell lysates were obtained by homogenizing MCs in RIPA buffer containing Roche complete protease inhibitors and passing them through a 26-gauge needle 10 times to disrupt the cells. The homogenates were centrifuged at 5000 rpm for 10 min at 4°C and supernatants used immediately or stored at - 80°C.

Transfection of small interfering RNA (siRNA) and recombinant adenovirus

Stealth™ negative universal control and TxNIP-specific Stealth™ RNAi oligonucleotides (Cat# TXNIPMSS285710) were obtained from Invitrogen. Reverse transfections were performed using the reagents and protocol from INTERFERin™ Polyplus transfection. Briefly, control siRNA (50nM) or TxNIP siRNA (50nM) was mixed with polyplus reagent and serum-free Opti-MEM (Invitrogen) for 20 min at room temperature. Two hundred µL were added to the C3H MC containing 1.8 mL of DMEM (10% FBS) and then incubated for 24h before growth arrest. The recombinant adenoviruses expressing green fluorescent protein (Ad-GFP) and TxNIP (Ad-TxNIP) were kindly provided by Dr. RT Lee, (Harvard, Boston). These viruses were amplified in 293A cells, purified and concentrated using the Vivapure AdenoPACK100 kit (Cedarlane). Experiments were conducted using stock titer of 10^9 infectious units (ifu)/ml. Briefly, a mixture containing DMEM with 15% FBS, 2.5mg/ml Poly-L-Lysine and adenovirus was added to sub-confluent Hcb19 MC and incubated for 24h before growth arrest. After preliminary dose-response experiments demonstrating levels of protein expression by immunoblotting (data not

shown), 250 µL of stock in 1.75mL media (25 x 10^7 ifu/10^6 cells to 1000 ul (10^9 ifu/10^6cells) were chosen for these studies.

Western Blotting

Protein concentrations in total cell lysates were determined using the modified Lowry microassay (Bio-Rad, Hercules, CA). After boiling in 4 x sample buffer, 20 µg protein were separated by 10-15% SDS-PAGE, transferred onto nitrocellulose membranes which were blocked with 5% milk-Tris buffered saline with 0.1% Tween 20 as described (34), using the following specific primary and secondary antibodies: Primary antibodies (1:1000): TxNIP (MBL), Nox2 and rac1 (Millipore), MnSOD and Prohibitin (Abcam), Nox4 (Novus), GPx1 (Epitomics), HO-1, Catalase, and Trx1 (Cell Signalling) and all others from Santa Cruz (β-actin 1:10,000). Secondary antibodies (1:4000): Anti-rabbit IgG HRP conjugate (Bio-Rad) and Peroxidase conjugated anti-mouse IgG (Jackson-Immuno Research Lab). Immunoblots were visualized by the ECL detection system (KPL Mandel Scientific) and the densitometric analyses were performed using NIH Image J software.

Quantitative real time RT-PCR

RNA was extracted using the RNeasy Mini kit (Qiagen), reverse transcribed with an Omniscript RT kit (Qiagen) using random primers in a total volume of 20µL according to the manufacturer's protocol. Real-time PCR using cDNA and SYBR Green PCR Master Mix (Applied Biosystems) was performed and analyzed on an ABI Prism 7900 HT Sequence Detection System (Applied Biosystem). The primers used were: Nox2 forward: 5'-TGATGTTAGTGGGAGCCGGGA TTG-3', Nox2 reverse: 5' TCTGCAAACCACTCAAAGGCATG-3'; Nox4 forward: 5' – GGATCACAGAAGGTCCCTAGCAG-3', Nox4 reverse: 5'-GCGGCTACATGCACACCT GAGAA-3'; and 18S forward: 5' – GGCTACCACATCCAAGGAA, 18S reverse: 5' – GCT GGAATTACCGCGGCT-3'. 18S RNA was used as the loading control. The relative amounts of mRNA were determined by the ΔΔ C_t calculations (35).

ROS and Mitochondrial Membrane Potential Measurement

MCs were cultured on glass coverslips and incubated in the dark with 1µM of carboxymethyl-H2-dichlorofluorescein diacetate (CM-H2-DCF-DA) or dihydroethidium (DHE) for 30 min at 37°C. Intracellular ROS production was assessed with an Olympus FluoView 1000 Laser Scanning Confocal Microscope, (ex/em λ=488nm/515nm for DCF; ex/em: 396nm/579nm for superoxide, and ex/em: 510nm /580nm for general ROS detection for DHE). Mitochondrial superoxide formation was detected by incubating cells in the dark with 5 µM MitoSOX Red dye (ex/em λ=510nm/580nm) for 30 min. To assess mitochondrial membrane potential, the cells were preincubated with 2µL/ml JC-1 dye (Invitrogen) for 30 min and detected at ex/em λ = 590/610 nm for JC-1 aggregates and ex/em λ 485/535 nm for monomers. The average fluorescence intensity per cell for each experimental group of cells was calculated using NIH Image J analysis software. An average of 10 cells/field and at least 4-5 random fields/condition were chosen for each experiment and analyzed in a blinded manner. Hydrogen peroxide released by the cells was assessed by incubating the growth media (phenol red-free) from the cells in a reaction mixture containing Amplex Red (Invitrogen) and then determining the absorbance at 560nm in a microplate-reader, as per the manufacturer's instruction. The readings were then normalized by the number of cells for each condition.

The rate of hydrogen peroxide disappearance in MCs was assessed according to Chen et al (40) with a slight modification. Briefly, growth arrested cells were pretreated with 10µM DPI (Diphenyleneiodonium chloride, Sigma) for 1h in order to inhibit endogenous NADPH oxidase and mitochondria derived ROS (37). Then different concentrations of H_2O_2 (hydrogen peroxide) (1µM-100µM) were added to the cells and the changes in the levels of ROS were measured at various intervals using CM-H2-DCF-DA dye and a Molecular Device plate

reader at ex/em λ 485/538 nm. Based on the results from preliminary experiments, the rates of ROS decomposition were linear between 120 and 180 min post H_2O_2 treatment; thus, the rates of ROS degradation under the various conditions were determined during this 1 h.

Mitochondria Isolation
MCs were harvested from the cultures and mitochondria were isolated using a Thermo Fisher Mitochondria isolation kit according to the instruction of the manufacturer.

Confocal Imaging of Collagen α (type IV)
MCs were cultured on glass coverslips and were treated with NG or HG for 24h after growth arrest. Cells were fixed in 3.7% formaldehyde, permeabilized in methanol and blocked with 1% goat serum plus 0.1% BSA. Immunofluorescence staining was performed by incubating the fixed cells with collagen α (IV) primary antibody(1:250, Rockland) and FITC-conjugated secondary antibody (1:100, BD Transduction Labs) and viewed with an Olympus Fluo View Confocal Microscope.

NADPH Oxidase Activity Assay
NADPH oxidase activity was measured using the lucigenin-enhanced chemiluminescence method as previously described (11). In brief, MCs were washed and homogenized in lysis buffer containing 20mM KH_2PO_4 (pH 7.0), 1mM EGTA and complete protease inhibitors (Roche Applied Science). A total of 100uL of homogenates were added to 900uL assay buffer comprising 50mM KH_2PO_4 (pH 7.0), 1mM EGTA, 150mM sucrose, 5uM lucigenin (electron acceptor) and 100uM NADPH (electron donor). Photo emission was measured every 30 seconds for 5 min with a GloMax luminometer. A buffer without NADPH was used as blank. Rate of superoxide generation was calculated by subtracting the readings from the blank and expressed as relative light units per min per mg protein.

Trx Activity Assay
After cell lysis, thioredoxin activity assay was performed according to Holmgren et al (38), with modifications. Briefly, duplicate samples of 50μg protein (from cell lysates) were added to 40μL of mixture 1 (400 μL 1M HEPES (pH 7.45), 160 μl 0.2 M EDTA, 120 μl NADPH (40 mg/mL), and 1000 μL insulin (10 mg/ml), bringing the final volume to 110 μL with water. To the first sample, 10 μL of Trx reductase was added, and to the second sample, 10 μL of water. The mixtures were incubated at 37°C for 20 min and the enzymatic activity was stopped by adding 250 μL stop buffer (6M Guanidine HCl and 0.4 mg/ml DNTB) to each tube. Two hundred uL from each tube was added to 96-well plates and readings were taken at 410 nm. The differences in the absorbance between Trx reductase and water treated samples represent the thioredoxin activity in the cell lysates.

Lactate Concentrations
Lactate concentrations in the cell culture media were assessed using the Abcam Lactate Colorimetric Assay kit according to the manufacturer's instruction.

Statistical Analysis
Results are expressed as means ± SE. Statistical analysis was performed by ANOVA followed by Newman–Keuls method for multiple comparisons using Graphpad Prism 4. Comparison between two sets of samples was analyzed by Student's t-test. $p< 0.05$ was considered to be statistically significant.

RESULTS
High glucose induces expression of collagen IV in wild-type C3H but not in TxNIP-deficient Hcb-19 mesangial cells. There is evidence in the literature demonstrating the effect of high glucose on the expression of TxNIP (39-41). In this study we verified that the primary mouse mesangial cells (MCs) harvested from C3H control mice exhibited a similar response. However, in Hcb-19 MC which lack TxNIP protein due to a spontaneous nonsense mutation in the gene encoding TxNIP (42), showed no expression by immunoblotting (Fig. 1A). Thus, treatment with high glucose resulted in a time-dependent increase in TxNIP which significantly increased in wild-type C3H MC by 1h of HG treatment, rising to ~15-fold by 24h (Fig. 1A).
One of the hallmarks of DN is increased mesangial ECM protein deposition (2,43).

Therefore, we determined whether TxNIP was required for this outcome. Collagen α (IV), an ECM protein known to be associated with glomerulosclerosis was increased 1.7±0.43 fold after 24h HG treatment of C3H MC, but no change was observed in Hcb-19 MC (Fig. 1B). These data, consistent with Kobayashi et al.'s findings (7), indicate that TxNIP is required for the induction of collagen IV protein by high glucose in MC.

TxNIP is required for the high glucose induced increase in MC ROS and decrease in Trx activity.

Intracellular ROS production was assessed by preincubating mesangial cells with a cell-permeable fluorescent probe, CM-H_2DCFDA that is oxidized to 2'7'-dichlorofluorescein by H_2O_2. As illustrated in Fig. 2A, HG-induced ROS production was augmented in C3H cells, peaking at 3h of treatment. However, HG exposure did not increase ROS in the Hcb-19 cells. Similar experiments were performed using dihyroethidium (DHE), another biomarker for cellular ROS. Fluorescent detection of superoxide production by the MC (Fig. 2B) was assessed at excitation/emission: 396/579 nm, and total ROS (Fig. 2C) that forms ethidium at 510/580 nm, as described (44). The pattern of superoxide and total ROS generation was similar to the results obtained from the DCF experiments (Fig. 2B-C). In order to confirm that the ROS signaling in C3H and Hcb19 cells (Figs. 2A-C) were not due to differences in the uptake of the dye by the different cells, the amount of H_2O_2 released was also assessed by the levels of resorufin (red-fluorescent oxidized product of Amplex Red reagent) in the cell culture media. As seen in Fig. 2D, the amount of H_2O_2 generated by the cells was similar to the ROS detected by DCF/DHE (Figs. 2A-C). Together, these data indicate that without TxNIP, there appears to be either an impairment in ROS generation or an increase in endogenous ROS scavenging/ antioxidant capacity.

To gain insight into the extent of Trx activity available to scavenge intracellular ROS, a Trx activity assay was performed using a modified version of the protocol of Holmgren et al (38). Interestingly, there was a significant reduction in the Trx activity in C3H MC by 1h of HG treatment that decreased by 69% (versus C3H NG) at 3h post treatment (Fig. 2E). This decline in the Trx activity, representing oxidation/ inactivation of endogenous Trx by the ROS and/or inhibition by TxNIP, could have partially accounted for the observed increase in ROS (Fig. 2A-D). On the other hand, although there was a trend towards a decrease in Trx activity in high glucose in Hcb-19 cells, the difference was not statistically significant.

H_2O_2 scavenging is not augmented in TxNIP deficient mesangial cells.

The lack of a significant decrease in endogenous Trx activity in TxNIP-deficient cells in the presence of high glucose was surprising and suggested that either there existed such an excess of antioxidant activity that a decrease was not detected, or that ROS generation was impaired. To more directly determine the ability of Hcb-19 MC to dissipate ROS, cells were exposed to 1μM and 10 μM H_2O_2 and ROS disappearance monitored over time by DCF fluorescence as described in Methods. The rate of disappearance of ROS was lower in Hcb-19 compared with C3H MC (Fig. 2F). These results appeared paradoxical since TxNIP is known to inhibit Trx and thus antioxidant activity. However, while Trx1 and 2 protein levels were minimally decreased in the basal state in Hcb-19 cells, they were rapidly upregulated (3h) in high glucose in C3H but not altered in Hcb-19 MC (Fig. 3). Together, these data suggested a defect in ROS generation in Hcb-19 cells.

High glucose-stimulated NADPH oxidase activity and Nox4 expression are impaired in Hcb-19 cells.

A significant source of high glucose stimulated ROS is NADPH oxidase. To investigate its role in the decreased ROS generation in TxNIP-deficiency, NADPH oxidase activity was measured before and after various times of high glucose exposure. Superoxide generation by the NADPH oxidase system was assessed by the lucigenin-enhanced chemiluminescence method in total cell lysates from MC treated with HG for 3h and 24h. NADPH oxidase activity was decreased in the basal state in the absence of TxNIP in Hcb-19 MC (Fig. 4A). After 3h of

HG exposure there was a 2.3±0.16 fold increase in the superoxide production in C3H MC that remained higher at 24h. In contrast, there were no significant changes in superoxide production in Hcb-19 cells after 3 or 24 h of HG (Fig. 4A). The two major isoforms of NADPH oxidase which are expressed in kidney are Nox2 and Nox4 with a small amount of Nox1 (4, 45). Indeed, Nox4, also known as "renox", is the most highly expressed. To investigate the contribution of Nox isoforms in the HG-induced NADPH oxidase activity, we determined their levels in the two cell types. Nox1 was only weakly detected, showed no difference between C3H and Hcb-19 MC and was not upregulated by HG (Fig. 5A). Nox2 was readily detected but also not different. We observed a trend towards increased Nox2 in HG in C3H MC but this did not reach statistical significance even after 24h (Fig. 4B). In addition, Nox2 mRNA was not altered by HG in either C3H or Hcb-19 MC (Fig. 4D). In contrast, Nox4 protein was lower in TxNIP deficient Hcb-19 MC in the basal state and not altered by HG, while in C3H Nox4 was rapidly induced (3h) and remained elevated at 24h (Fig. 4C). Similar results were obtained by real-time RT-PCR assessment of Nox4 mRNA, which was increased by HG only in C3H MC (Fig.4E). The increase in NADPH oxidase activity stimulated by HG has also been associated with upregulation of other Nox-associated subunits such as $p47^{phox}$, $p67^{phox}$, rac1 and $p22^{phox}$ (4, 13, 15, 46, 47). While $p22^{phox}$ could contribute to Nox2 and/or Nox4, the former 3 proteins are associated with Nox2 activity (4, 45, 48, 49). Under these conditions there was a significant but transient increase in $p47^{phox}$ induced by HG in C3H which returned to basal levels after 24h. However, there was no change detected in Hcb-19 (Fig. 5B). Similarly, there were no changes caused by HG in $p67^{phox}$ or rac1 in either cell type (Fig. 5C and 5D). $p22^{phox}$ was also significantly induced by HG only in C3H MC, and this increase was maintained at 24h (Fig. 5E). Thus, while we cannot rule out a contribution to the HG-stimulated NADPH oxidase activity of Nox2 at 3h, these data suggest that Nox4 is the major isoform involved, particularly at 24h. In addition, TxNIP is necessary for upregulation of Nox4 as well as the subunits, $p47^{phox}$ and $p22^{phox}$ in HG.

High glucose promotes ROS production and Nox4 protein expression in the mitochondria of C3H MC.

There are studies that have demonstrated that Nox4 siRNA or antisense oligonucleotides block high glucose-induced increases in mesangial cell ROS, i.e. cytosolic NADPH oxidase activity as well as mitochondrial superoxide formation, indicating that Nox4 is essential for HG-induced MC ROS generation (14, 16). These findings are also consistent with the observation that Nox4 is an important mediator of mesangial matrix accumulation in diabetes (14).

To examine mitochondria specific ROS generation and Nox4 expression, MC were treated with HG for varying times and superoxide generation in live cells was measured with MitoSOX Red , a mitochondria specific fluorogenic dye that produces red fluorescence upon being oxidized by superoxide. By 1h of HG treatment, there was a significant rise in mitochondrial superoxide production in C3H MC which remained elevated up to 24h of HG treatment (Fig. 6A). However, mitochondrial ROS production by Hcb-19 MC was not affected by HG (Fig. 6A), indicating mitochondrial dysfunction, at least in this respect, in Hcb-19 cells lacking TxNIP.

In MC, Nox4 has been found to primarily localize to mitochondria and to a lesser extent to plasma membranes (16). Thus, the expression of Nox4 in mitochondrial extracts from HG-treated MCs was examined. The mitochondrial fractions were prepared as described in Methods and purity verified by immunoblotting of the mitochondrial markers prohibitin, COX IV and VDAC/porin (Fig. 6B). As shown in Fig. 6C, there was a dramatic increase in Nox4 levels in HG treated C3H cells, but in Hcb-19, mitochondrial Nox4 expression remained unaffected. Therefore, it appears that TxNIP plays an important role in inducing mitochondrial Nox4, which in turn contributes to the ROS production.

Knockdown of TxNIP in wild-type C3H MC

mimics the features of Hcb-19 cells. To verify that the defects in ROS generation, NADPH oxidase activation and Nox4 expression upon HG exposure in TxNIP-deficient Hcb-19 MC were caused by the lack of TxNIP, the wild-type C3H cells were treated with TxNIP-specific or scrambled siRNA. TxNIP protein was effectively decreased upon knockdown with siRNA in HG to levels even below that of scrambled siRNA transfected cells and completely blocked the upregulation of TxNIP by HG (Fig. 7D). This decrease in TxNIP markedly inhibited HG-stimulated cellular ROS monitored by DCF fluorescence (Fig. 7A), mitochondria-specific ROS detected with MitoSox (Fig.7B) and NADPH oxidase activity (Fig.7C). In addition TxNIP knockdown blocked Nox4 induction (Fig. 7D) in response to HG and collagen IV accumulation, an *in vitro* marker of the increased ECM protein in DN (Fig. 7E). These results in C3H cells with TxNIP-specific knockdown indicate the requirement of TxNIP as a mediator of HG signalling.

Overexpression of TxNIP in Hcb-19 MC augments mitochondrial ROS and Nox4. To confirm the functional role of TxNIP in HG signalling, the TxNIP-deficient Hcb-19 MC were transduced with TxNIP expressing adenovirus (AdTxNIP) or control GFP expressing adenovirus (AdGFP). Dose-response experiments revealed that $25x10^7$ ifu (infectious units)/ml/well (10^6 cells) for 24h resulted in TxNIP protein levels that were at least as high as those observed after HG exposure of C3H MC (Fig. 8B and Fig. 1A). Mitochondrial O2·– production was then examined in normal and HG. As expected, HG stimulated mitochondrial O2·– in control AdGFP transfected C3H MC (1.96 ± 0.22 fold of NG, $p< 0.05$) but not in AdGFP Hcb-19 (Fig. 8A). However, AdTxNIP transfected Hcb-19 cells showed increased MitoSox fluorescence in normal glucose (~2-fold of AdGFP Hcb-19) which did not increase further with HG treatment (Fig. 8A). Measurement of Nox4 protein showed a TxNIP dose-dependent increase in Hcb-19 cells in normal glucose which also did not increase further in HG (Fig. 8B).These data indicate that TxNIP, when expressed at levels similar to that observed with HG in MC, induces mitochondrial ROS and Nox4 expression and support the notion that it plays a key role in diabetic nephropathy.

TxNIP is required for the high glucose-associated increase in mitochondrial/TCA cycle glucose metabolism.
TxNIP has been recently implicated as a "gatekeeper" of pyruvate conversion to acetylCoA for mitochondrial glucose oxidation via the TCA cycle and electron transport (50). Cardiomyocytes from $TxNIP^{-/-}$ mice display increased glycolysis and lactate production, a Warburg-like effect (50). Evidence for this metabolic pattern was observed in Hcb-19 MC in which exposure to HG resulted in a significant elevation of lactate concentrations in the medium that was not observed in C3H (Fig. 9A).

Glucose metabolite flux and oxidation in mitochondria was assessed by measuring the mitochondrial membrane potential (MMP). MMP is increased by flux through the electron transport chain and generation of a proton gradient across the membrane (51). JC-1 is a cationic dye that selectively enters and accumulates in mitochondrial matrix, where it forms J-aggregates with intense red fluorescence upon exceeding critical concentrations, thereby changing its color from green to red as the membrane potential is increased (52). In control C3H MC, mitochondrial membrane potential increased when HG was added forming red JC-1 aggregates (Fig 9B, upper panel). In contrast, in Hcb-19 cells, JC-1 remained in its monomeric form as shown by green fluorescence (Fig 9B, lower panel), indicating that mitochondrial glucose metabolism was not augmented in these cells. These results support the concept that TxNIP plays a key role augmenting glucose metabolic flux via the TCA cycle and that the defects in HG signalling may be mediated, at least in part, by this deficiency in mitochondrial function.

DISCUSSION

The importance of elevated levels of ROS in the pathogenesis of the microvascular complications of diabetes has been well documented (11, 12,

53). While increased mitochondrial glucose oxidation and flux through the electron transport chain have been suggested to be the primary source, elevated NADPH oxidase activity has also been demonstrated to contribute to increased ROS and ultimately, to the pro-fibrotic signalling in the kidney stimulated by hyperglycemia (11-15). The cellular levels of ROS and the presence of oxidative stress are determined not only by rates of ROS generation, but also their neutralization and degradation by endogenous antioxidants. It has been proposed that by binding to and inhibiting the antioxidant Trxs, TxNIP upregulation by HG promotes oxidative stress (27, 54). A specific role in the kidney was suggested by Kobayashi et al who showed that overexpression of TxNIP in cultured MC led to increased collagen IV mRNA and protein (7). A truncated TxNIP mutant which failed to bind Trx lacked this effect (7). In this study, we found a rapid, marked and sustained upregulation of TxNIP in primary cultures of wild-type C3H MC exposed to HG. This was associated with increased production of ROS and collagen accumulation. In contrast, in Hcb-19 TxNIP-deficient MC, exposure to HG did not stimulate ROS or increase collagen. We reasoned that the inhibition of Trx in HG by augmented TxNIP would limit the dissipation of ROS and promote oxidative stress and that an absence of TxNIP would permit more effective antioxidant neutralizing capacity. However, in the Hcb-19 MC the TxNIP deficiency was associated with a lack of response to HG of NADPH oxidase activity and upregulation of the major renal NADPH oxidase isoform, Nox4. These data indicated a defect in ROS generation. Indeed, direct assessment of H_2O_2 dissipation in the two MC lines revealed that in contrast to what was expected, ROS degradation was decreased in the absence of TxNIP. In the Hcb-19 MC, the protein content of several endogenous antioxidant enzymes including Trx1, Trx2, catalase and HO-1 (hemoxygenase-1) tended to be lower in the basal state and showed no increase in HG in contrast to C3H MC (Fig.3). While we cannot rule out a contribution of Nox2 to the HG-induced NADPH oxidase activity in C3H MC, the lack of upregulation of $p47^{phox}$ and $p22^{phox}$ in Hcb-19 MC (Fig. 5) would also be consistent with an absent NADPH oxidase response to HG without TxNIP.

The mechanism of upregulation of Nox4 by HG is not clear. However, there are multiple stimulatory transcriptional regulators including NFkB, HIF1-α, AP-1 and Nrf-2 (55-59), which may all be activated by HG (10, 11, 60). Under basal conditions, Trx in mitochondria binds and inhibits ASK (Apoptosis signal-regulating kinase)-1, an upstream MKK3/6 and p38 MAPK activator (61 - 63). TxNIP upregulation has been proposed to bind Trx and release ASK-1 to activate p38 (64 - 66), which in turn would stimulate AP-1 (67, 68). In support of this possibility, TxNIP has recently been reported to translocate to the mitochondria in the presence of ROS in pancreatic β-cells (65). It has also been found that NF-kB transcriptional activation requires ROS (69) and NFkB is activated in response to HG in endothelial cells (70). Recently, the activation of Nrf-2 in response to the increased ROS induced by HG has been documented and appears to be a negative feedback, protective pathway by inducing an antioxidant response (71). The lack of upregulation of enzymes such as HO-1, a Nrf-2 responsive gene, in Hcb-19 MC in HG is consistent with the absence of ROS generation.

Since ROS are well documented cell signalling molecules, it is not clear whether the defect(s) observed in NADPH oxidase activation is primary or secondary. In this context, we examined mitochondria-specific ROS generation using MitoSox. In contrast to controls, in the absence of TxNIP, there was no increase in mitochondrial ROS ($O_2^{\cdot-}$) in response to HG in Hcb-19 MC. The key role of TxNIP was demonstrated by reproducing these defects in wild-type C3H MC using TxNIP-specific siRNA-mediated knockdown (Fig. 7). Thus, decreased total cellular ROS and mitochondrial $O_2^{\cdot-}$ associated with decreased NADPH oxidase activity, Nox4 and collagen expression, were documented in response to HG in C3H MC with TxNIP knockdown compared to C3H MC transfected with scrambled siRNA. Furthermore, restoration of TxNIP by adenoviral expression induced mitochondrial ROS and Nox4 expression in Hcb-19 cells even in the

absence of HG.

Increased mitochondria-derived ROS in response to HG has been proposed to act as an initiator of the alterations in glucose metabolic pathways that contribute to the complications of diabetes (9 - 11). Thus, a relevant action of TxNIP could be its recently appreciated function to regulate glucose metabolism, specifically to increase mitochondrial glucose oxidation (50). In cardiomyocytes, protection from ischaemia-reperfusion injury in intact hearts from TxNIP$^{-/-}$ mice was associated with increased glycolysis to lactate and a defect in entry of pyruvate into the Krebs' cycle (50). In HG, increased mitochondrial glucose oxidation is observed and we found a marked increase in the mitochondrial membrane potential in C3H MC exposed to HG. However, this increase was completely absent in TxNIP deficient Hcb-19 MC (Fig. 9) and was accompanied by an increase in lactate. These data in MC are similar to the glucose metabolic phenotype reported in cardiomyocytes and are consistent with a primary mitochondrial defect in ROS generation. It is not clear whether this metabolic effect is mediated by the Trx binding site of TxNIP or possibly, by its α-arrestin domain (72).

In summary, this study demonstrates widespread defects in ROS generation in response to HG in MC which lack TxNIP, from both mitochondria and NADPH oxidase(s). Although TxNIP inhibits the endogenous antioxidant Trx, the decrease in ROS is not due to more rapid degradation of these reactive molecules, but appears to be mediated, at least in part, by a defect in regulating glucose metabolic flux to the TCA cycle. While we cannot exclude other direct actions of TxNIP which binds various proteins (73 - 75), this defect in mitochondrial and Nox4-mediated ROS generation would inhibit multiple signalling pathways such as PKC, AGE formation, O-glycosylation and TGF-β1, activated by high glucose. Thus, the lack of TxNIP was associated with protection from the pro-fibrotic signalling to collagen expression by HG. In view of the marked upregulation of TxNIP and the key signalling role of ROS in HG-induced microvascular complications, TxNIP may be a relevant and powerful novel therapeutic target in their treatment and prevention.

ACKNOWLEDGEMENTS

This work was supported by grants from the Canadian Institutes of Health Research (CIHR) (MOP 97979 and PCN 49409) to IGF. AS was supported in part by a Novo Nordisk Studentship from the Banting and Best Diabetes Centre; a Canada Graduate Scholarship (NSERC) and an Ontario Graduate Scholarship. KL was supported in part by a Novo Nordisk Studentship from the Banting and Best Diabetes Centre and from the Canadian Diabetes Association (Grant No OG-3-10-2997-IF). The authors thank Dr. R. Lee for reagents and helpful discussion.

REFERENCES

1.The Diabetes Control and Complications Trial Research Group. (1993) The effect of intensive treatment of diabetes on the development and progression of long-term complications in insulin-dependent diabetes mellitus. *N. Engl. J. Med.* **329**, 977-986

2.Molitch, M. E., DeFronzo, R. A., Franz, M. J., Keane, W. F., Mogensen, C. E., Parving, H. H., and Steffes, M. W. (2004) Nephropathy in diabetes. *Diabetes Care* **27 Suppl 1**, S79-83

3.Dronavalli, S., Duka, I., and Bakris, G. L. (2008) The pathogenesis of diabetic nephropathy. *Nat. Clin. Pract. Endocrinol. Metab.* **4**, 444-452

4.Kakehi, T., and Yabe-Nishimura, C. (2008) NOX enzymes and diabetic complications. *Semin. Immunopathol.* **30**, 301-314

5.Kanwar, Y. S., Wada, J., Sun, L., Xie, P., Wallner, E. I., Chen, S., Chugh, S., and Danesh, F. R. (2008) Diabetic nephropathy: mechanisms of renal disease progression. *Exp. Biol. Med. (Maywood)* **233**, 4-11

6.Lee, H. B., Yu, M. R., Yang, Y., Jiang, Z., and Ha, H. (2003) Reactive oxygen species-regulated signaling pathways in diabetic

nephropathy. *J. Am. Soc. Nephrol.* **14**, S241-245

7.Kobayashi, T., Uehara, S., Ikeda, T., Itadani, H., and Kotani, H. (2003) Vitamin D3 up-regulated protein-1 regulates collagen expression in mesangial cells. *Kidney Int.* **64**, 1632-1642

8.Shankland, S. J. (2006) The podocyte's response to injury: role in proteinuria and glomerulosclerosis. *Kidney Int.* **69**, 2131-2147

9.Brownlee, M. (2005) The pathobiology of diabetic complications: a unifying mechanism. *Diabetes* **54**, 1615-1625

10.Nishikawa, T., Edelstein, D., Du, X. L., Yamagishi, S., Matsumura, T., Kaneda, Y., Yorek, M. A., Beebe, D., Oates, P. J., Hammes, H. P., Giardino, I., and Brownlee, M. (2000) Normalizing mitochondrial superoxide production blocks three pathways of hyperglycaemic damage. *Nature* **404**, 787-790

11.Giacco, F., and Brownlee, M. (2010) Oxidative stress and diabetic complications. *Circ. Res.* **107**, 1058-1070

12.Forbes, J. M., Coughlan, M. T., and Cooper, M. E. (2008) Oxidative stress as a major culprit in kidney disease in diabetes. *Diabetes* **57**, 1446-1454

13.Xia, L., Wang, H., Goldberg, H. J., Munk, S., Fantus, I. G., and Whiteside, C. I. (2006) Mesangial cell NADPH oxidase upregulation in high glucose is protein kinase C dependent and required for collagen IV expression. *Am. J. Physiol. Renal Physiol.* **290**, F345-356

14.Gorin, Y., Block, K., Hernandez, J., Bhandari, B., Wagner, B., Barnes, J. L., and Abboud, H. E. (2005) Nox4 NAD(P)H oxidase mediates hypertrophy and fibronectin expression in the diabetic kidney. *J. Biol. Chem.* **280**, 39616-39626

15.Thallas-Bonke, V., Thorpe, S. R., Coughlan, M. T., Fukami, K., Yap, F. Y., Sourris, K. C., Penfold, S. A., Bach, L. A., Cooper, M. E., and Forbes, J. M. (2008) Inhibition of NADPH oxidase prevents advanced glycation end product-mediated damage in diabetic nephropathy through a protein kinase C-alpha-dependent pathway. *Diabetes* **57**, 460-469

16.Block, K., Gorin, Y., and Abboud, H. E. (2009) Subcellular localization of Nox4 and regulation in diabetes. *Proc. Natl. Acad. Sci. U.S.A.* **106**, 14385-14390

17.Chacko, B. K., Reily, C., Srivastava, A., Johnson, M. S., Ye, Y., Ulasova, E., Agarwal, A., Zinn, K. R., Murphy, M. P., Kalyanaraman, B., and Darley-Usmar, V. (2010) Prevention of diabetic nephropathy in Ins2(+/)(AkitaJ) mice by the mitochondria-targeted therapy MitoQ. *Biochem. J.* **432**, 9-19

18.Fujita, H., Fujishima, H., Chida, S., Takahashi, K., Qi, Z., Kanetsuna, Y., Breyer, M. D., Harris, R. C., Yamada, Y., and Takahashi, T. (2009) Reduction of renal superoxide dismutase in progressive diabetic nephropathy. *J. Am. Soc. Nephrol.* **20**, 1303-1313

19.Hamada, Y., Miyata, S., Nii-Kono, T., Kitazawa, R., Kitazawa, S., Higo, S., Fukunaga, M., Ueyama, S., Nakamura, H., Yodoi, J., Fukagawa, M., and Kasuga, M. (2007) Overexpression of thioredoxin1 in transgenic mice suppresses development of diabetic nephropathy. *Nephrol. Dial. Transplant.* **22**, 1547-1557

20.Sedeek, M., Callera, G., Montezano, A., Gutsol, A., Heitz, F., Szyndralewiez, C., Page, P., Kennedy, C. R., Burns, K. D., Touyz, R. M., and Hebert, R. L. (2010) Critical role of Nox4-based NADPH oxidase in glucose-induced oxidative stress in the kidney: implications in type 2 diabetic nephropathy. *Am. J. Physiol. Renal Physiol.* **299**, F1348-1358

21.Cheng, D. W., Jiang, Y., Shalev, A., Kowluru, R., Crook, E. D., and Singh, L. P. (2006) An analysis of high glucose and glucosamine-induced gene expression and oxidative stress in renal mesangial cells. *Arch. Physiol. Biochem.* **112**, 189-218

22.Parikh, H., Carlsson, E., Chutkow, W. A.,

Johansson, L. E., Storgaard, H., Poulsen, P., Saxena, R., Ladd, C., Schulze, P. C., Mazzini, M. J., Jensen, C. B., Krook, A., Bjornholm, M., Tornqvist, H., Zierath, J. R., Ridderstrale, M., Altshuler, D., Lee, R. T., Vaag, A., Groop, L. C., and Mootha, V. K. (2007) TXNIP regulates peripheral glucose metabolism in humans. *PLoS Med.* **4**, e158

23.Shalev, A., Pise-Masison, C. A., Radonovich, M., Hoffmann, S. C., Hirshberg, B., Brady, J. N., and Harlan, D. M. (2002) Oligonucleotide microarray analysis of intact human pancreatic islets: identification of glucose-responsive genes and a highly regulated TGFbeta signaling pathway. *Endocrinology* **143**, 3695-3698

24.Chen, K. S., and DeLuca, H. F. (1994) Isolation and characterization of a novel cDNA from HL-60 cells treated with 1,25-dihydroxyvitamin D-3. *Biochim. Biophys. Acta.* **1219**, 26-32

25.Miranda-Vizuete, A., Damdimopoulos, A. E., Gustafsson, J., and Spyrou, G. (1997) Cloning, expression, and characterization of a novel Escherichia coli thioredoxin. *J. Biol. Chem.* **272**, 30841-30847

26.Patwari, P., Higgins, L. J., Chutkow, W. A., Yoshioka, J., and Lee, R. T. (2006) The interaction of thioredoxin with Txnip. Evidence for formation of a mixed disulfide by disulfide exchange. *J. Biol. Chem.* **281**, 21884-21891

27.Schulze, P. C., Yoshioka, J., Takahashi, T., He, Z., King, G. L., and Lee, R. T. (2004) Hyperglycemia promotes oxidative stress through inhibition of thioredoxin function by thioredoxin-interacting protein. *J. Biol. Chem.* **279**, 30369-30374

28.Masson, E., Koren, S., Razik, F., Goldberg, H., Kwan, E. P., Sheu, L., Gaisano, H. Y., and Fantus, I. G. (2009) High beta-cell mass prevents streptozotocin-induced diabetes in thioredoxin-interacting protein-deficient mice. *Am. J. Physiol. Endocrinol. Metab.* **296**, E1251-1261

29.Chen, J., Hui, S. T., Couto, F. M., Mungrue, I. N., Davis, D. B., Attie, A. D., Lusis, A. J., Davis, R. A., and Shalev, A. (2008) Thioredoxin-interacting protein deficiency induces Akt/Bcl-xL signaling and pancreatic beta-cell mass and protects against diabetes. *FASEB J.* **22**, 3581-3594

30.Chen, J., Fontes, G., Saxena, G., Poitout, V., and Shalev, A. (2010) Lack of TXNIP protects against mitochondria-mediated apoptosis but not against fatty acid-induced ER stress-mediated beta-cell death. *Diabetes* **59**, 440-447

31.Minn, A. H., Hafele, C., and Shalev, A. (2005) Thioredoxin-interacting protein is stimulated by glucose through a carbohydrate response element and induces beta-cell apoptosis. *Endocrinology* **146**, 2397-2405

32.Mene, P., and Stoppacciaro, A. (2009) Isolation and propagation of glomerular mesangial cells. *Methods Mol. Biol.* **466**, 3-17

33.Takemoto, M., Asker, N., Gerhardt, H., Lundkvist, A., Johansson, B. R., Saito, Y., and Betsholtz, C. (2002) A new method for large scale isolation of kidney glomeruli from mice. *Am. J. Pathol.* **161**, 799-805

34.Beard, K. M., Lu, H., Ho, K., and Fantus, I. G. (2006) Bradykinin augments insulin-stimulated glucose transport in rat adipocytes via endothelial nitric oxide synthase-mediated inhibition of Jun NH2-terminal kinase. *Diabetes* **55**, 2678-2687

35.Livak, K. J., and Schmittgen, T. D. (2001) Analysis of relative gene expression data using real-time quantitative PCR and the 2(-Delta Delta C(T)) Method. *Methods* **25**, 402-408

36.Chen, J., Chen, J. K., Nagai, K., Plieth, D., Tan, M., Lee, T. C., Threadgill, D. W., Neilson, E. G., and Harris, R. C. (2012) EGFR signaling promotes TGFbeta-dependent renal fibrosis. *J. Am. Soc. Nephrol.* **23**, 215-224

37.Li, Y., and Trush, M. A. (1998) Diphenyleneiodonium, an NAD(P)H oxidase inhibitor, also potently inhibits mitochondrial reactive oxygen species production. *Biochem.*

Biophys. Res. Commun. **253**, 295-299

38.Bjornstedt, M., Kumar, S., and Holmgren, A. (1995) Selenite and selenodiglutathione: reactions with thioredoxin systems. *Methods Enzymol.* **252**, 209-219

39.Zitman-Gal, T., Green, J., Pasmanik-Chor, M., Oron-Karni, V., and Bernheim, J. (2010) Endothelial pro-atherosclerotic response to extracellular diabetic-like environment: possible role of thioredoxin-interacting protein. *Nephrol. Dial. Transplant.* **25**, 2141-2149

40.Chen, J., Saxena, G., Mungrue, I. N., Lusis, A. J., and Shalev, A. (2008) Thioredoxin-interacting protein: a critical link between glucose toxicity and beta-cell apoptosis. *Diabetes* **57**, 938-944

41.Cha-Molstad, H., Saxena, G., Chen, J., and Shalev, A. (2009) Glucose-stimulated expression of Txnip is mediated by carbohydrate response element-binding protein, p300, and histone H4 acetylation in pancreatic beta cells. *J. Biol. Chem.* **284**, 16898-16905

42.Bodnar, J. S., Chatterjee, A., Castellani, L. W., Ross, D. A., Ohmen, J., Cavalcoli, J., Wu, C., Dains, K. M., Catanese, J., Chu, M., Sheth, S. S., Charugundla, K., Demant, P., West, D. B., de Jong, P., and Lusis, A. J. (2002) Positional cloning of the combined hyperlipidemia gene Hyplip1. *Nat. Genet.* **30**, 110-116

43.Balakumar, P., Arora, M. K., Reddy, J., and Anand-Srivastava, M. B. (2009) Pathophysiology of diabetic nephropathy: involvement of multifaceted signalling mechanism. *J. Cardiovasc. Pharmacol.* **54**, 129-138

44.Spencer, N. Y., Yan, Z., Boudreau, R. L., Zhang, Y., Luo, M., Li, Q., Tian, X., Shah, A. M., Davisson, R. L., Davidson, B., Banfi, B., and Engelhardt, J. F. (2011) Control of hepatic nuclear superoxide production by glucose 6-phosphate dehydrogenase and NADPH oxidase-4. *J. Biol. Chem.* **286**, 8977-8987

45.Lambeth, J. D., Kawahara, T., and Diebold, B. (2007) Regulation of Nox and Duox enzymatic activity and expression. *Free Radic. Biol. Med.* **43**, 319-331

46.Kitada, M., Koya, D., Sugimoto, T., Isono, M., Araki, S., Kashiwagi, A., and Haneda, M. (2003) Translocation of glomerular p47phox and p67phox by protein kinase C-beta activation is required for oxidative stress in diabetic nephropathy. *Diabetes* **52**, 2603-2614

47.Li, J., Zhu, H., Shen, E., Wan, L., Arnold, J. M., and Peng, T. (2010) Deficiency of rac1 blocks NADPH oxidase activation, inhibits endoplasmic reticulum stress, and reduces myocardial remodeling in a mouse model of type 1 diabetes. *Diabetes* **59**, 2033-2042

48.Martyn, K. D., Frederick, L. M., von Loehneysen, K., Dinauer, M. C., and Knaus, U. G. (2006) Functional analysis of Nox4 reveals unique characteristics compared to other NADPH oxidases. *Cell Signal.* **18**, 69-82

49.Serrander, L., Cartier, L., Bedard, K., Banfi, B., Lardy, B., Plastre, O., Sienkiewicz, A., Forro, L., Schlegel, W., and Krause, K. H. (2007) NOX4 activity is determined by mRNA levels and reveals a unique pattern of ROS generation. *Biochem. J.* **406**, 105-114

50.Yoshioka, J., Chutkow, W. A., Lee, S., Kim, J. B., Yan, J., Tian, R., Lindsey, M. L., Feener, E. P., Seidman, C. E., Seidman, J. G., and Lee, R. T. (2012) Deletion of thioredoxin-interacting protein in mice impairs mitochondrial function but protects the myocardium from ischemia-reperfusion injury. *J. Clin. Invest.* **122**, 267-279

51.Perry, S. W., Norman, J. P., Barbieri, J., Brown, E. B., and Gelbard, H. A. (2011) Mitochondrial membrane potential probes and the proton gradient: a practical usage guide. *Biotechniques* **50**, 98-115

52.Mathur, A., Hong, Y., Kemp, B. K., Barrientos, A. A., and Erusalimsky, J. D. (2000) Evaluation of fluorescent dyes for the detection of mitochondrial membrane potential changes in cultured cardiomyocytes. *Cardiovasc. Res.* **46**, 126-138

53.Singh, D. K., Winocour, P., and Farrington, K. (2011) Oxidative stress in early diabetic nephropathy: fueling the fire. *Nat. Rev. Endocrinol.* **7**, 176-184

54.Li, X., Rong, Y., Zhang, M., Wang, X. L., LeMaire, S. A., Coselli, J. S., Zhang, Y., and Shen, Y. H. (2009) Up-regulation of thioredoxin interacting protein (Txnip) by p38 MAPK and FOXO1 contributes to the impaired thioredoxin activity and increased ROS in glucose-treated endothelial cells. *Biochem. Biophys. Res. Commun.* **381**, 660-665

55.Zhang, L., Sheppard, O. R., Shah, A. M., and Brewer, A. C. (2008) Positive regulation of the NADPH oxidase NOX4 promoter in vascular smooth muscle cells by E2F. *Free Radic. Biol.Med.* **45**, 679-685

56.Manea, A., Tanase, L. I., Raicu, M., and Simionescu, M. (2010) Transcriptional regulation of NADPH oxidase isoforms, Nox1 and Nox4, by nuclear factor-kappaB in human aortic smooth muscle cells. *Biochem. Biophys. Res. Commun.* **396**, 901-907

57.Manea, A., Manea, S. A., Gafencu, A. V., Raicu, M., and Simionescu, M. (2008) AP-1-dependent transcriptional regulation of NADPH oxidase in human aortic smooth muscle cells: role of p22phox subunit. *Arterioscler. Thromb. Vasc. Biol.* **28**, 878-885

58.Diebold, I., Petry, A., Hess, J., and Gorlach, A. (2010) The NADPH oxidase subunit NOX4 is a new target gene of the hypoxia-inducible factor-1. *Mol. Biol. Cell.* **21**, 2087-2096

59.Pendyala, S., Moitra, J., Kalari, S., Kleeberger, S. R., Zhao, Y., Reddy, S. P., Garcia, J. G., and Natarajan, V. (2011) Nrf2 regulates hyperoxia-induced Nox4 expression in human lung endothelium: identification of functional antioxidant response elements on the Nox4 promoter. *Free Radic. Biol. Med.* **50**, 1749-1759

60.He, X., Kan, H., Cai, L., and Ma, Q. (2009) Nrf2 is critical in defense against high glucose-induced oxidative damage in cardiomyocytes. *J. Mol. Cell. Cardiol.* **46**, 47-58

61.Zhang, R., Al-Lamki, R., Bai, L., Streb, J. W., Miano, J. M., Bradley, J., and Min, W. (2004) Thioredoxin-2 inhibits mitochondria-located ASK1-mediated apoptosis in a JNK-independent manner. *Circ. Res.* **94**, 1483-1491

62.Fujino, G., Noguchi, T., Matsuzawa, A., Yamauchi, S., Saitoh, M., Takeda, K., and Ichijo, H. (2007) Thioredoxin and TRAF family proteins regulate reactive oxygen species-dependent activation of ASK1 through reciprocal modulation of the N-terminal homophilic interaction of ASK1. *Mol. Cell. Biol.* **27**, 8152-8163

63.Hattori, K., Naguro, I., Runchel, C., and Ichijo, H. (2009) The roles of ASK family proteins in stress responses and diseases. *Cell. Commun. Signal.* **7**, 9

64.Yamawaki, H., Pan, S., Lee, R. T., and Berk, B. C. (2005) Fluid shear stress inhibits vascular inflammation by decreasing thioredoxin-interacting protein in endothelial cells. *J. Clin. Invest.* **115**, 733-738

65.Saxena, G., Chen, J., and Shalev, A. (2010) Intracellular shuttling and mitochondrial function of thioredoxin-interacting protein. *J. Biol. Chem.* **285**, 3997-4005

66.Chen, C. L., Lin, C. F., Chang, W. T., Huang, W. C., Teng, C. F., and Lin, Y. S. (2008) Ceramide induces p38 MAPK and JNK activation through a mechanism involving a thioredoxin-interacting protein-mediated pathway. *Blood* **111**, 4365-4374

67.Lv, Z. M., Wang, Q., Wan, Q., Lin, J. G., Hu, M. S., Liu, Y. X., and Wang, R. (2011) The role of the p38 MAPK signaling pathway in high glucose-induced epithelial-mesenchymal transition of cultured human renal tubular epithelial cells. *PLoS One* **6**, e22806

68.Lan, T., Liu, W., Xie, X., Xu, S., Huang, K., Peng, J., Shen, X., Liu, P., Wang, L., Xia, P., and Huang, H. (2011) Sphingosine kinase-1

pathway mediates high glucose-induced fibronectin expression in glomerular mesangial cells. *Mol. Endocrinol.* **25**, 2094-2105

69.Gloire, G., Legrand-Poels, S., and Piette, J. (2006) NF-kappaB activation by reactive oxygen species: fifteen years later. *Biochem. Pharmacol.* **72**, 1493-1505

70.Yang, W. S., Seo, J. W., Han, N. J., Choi, J., Lee, K. U., Ahn, H., Lee, S. K., and Park, S. K. (2008) High glucose-induced NF-kappaB activation occurs via tyrosine phosphorylation of IkappaBalpha in human glomerular endothelial cells: involvement of Syk tyrosine kinase. *Am. J. Physiol. Renal Physiol.* **294**, F1065-1075

71.Li, H., Wang, F., Zhang, L., Cao, Y., Liu, W., Hao, J., Liu, Q., and Duan, H. (2011) Modulation of Nrf2 expression alters high glucose-induced oxidative stress and antioxidant gene expression in mouse mesangial cells. *Cell. Signal.* **23**, 1625-1632

72.Patwari, P., Chutkow, W. A., Cummings, K., Verstraeten, V. L., Lammerding, J., Schreiter, E. R., and Lee, R. T. (2009) Thioredoxin-independent regulation of metabolism by the alpha-arrestin proteins. *J. Biol. Chem.* **284**, 24996-25003

73.Jeon, J. H., Lee, K. N., Hwang, C. Y., Kwon, K. S., You, K. H., and Choi, I. (2005) Tumor suppressor VDUP1 increases p27(kip1) stability by inhibiting JAB1. *Cancer Res.* **65**, 4485-4489

74.Zhou, R., Tardivel, A., Thorens, B., Choi, I., and Tschopp, J. (2010) Thioredoxin-interacting protein links oxidative stress to inflammasome activation. *Nat. Immunol.* **11**, 136-140

75. Lee, S., Kim, S.M., and Lee, R.T. (June, 2012) Thioredoxin and thioredoxin target proteins: from molecular mechanisms to functional significance. Antioxid. Redox Signal. 10.1089/ARS.2011.4322.

ABBREVIATIONS

thioredoxin-interacting protein (TxNIP)
reactive oxygen species (ROS)
diabetic nephropathy (DN)
mesangial cells (MC)
extracellular matrix (ECM)
O2·–(superoxide)
glyceraldehyde -3- phosphate dehydrogenase (GAPDH)
diacylglycerol (DAG)
hexosamine biosynthetic pathway (HBP)
superoxide dismutase (SOD)
thioredoxins (Trx)
dihyroethidium (DHE)
glutathione peroxidase (Gpx)
Manganese-dependent superoxide dismutase (MnSOD)
Heme oxygenase-1 (HO-1)

FIGURE LEGENDS

FIGURE 1. **High glucose (HG)-stimulated collagen accumulation is impaired in Hcb-19 TxNIP-deficient mesangial cells (MC).** Growth arrested MC (C3H, Hcb-19) were exposed to NG (5.6mM) or HG (25mM) for up to 24h. **A**: Proteins from total cell lysates were separated on SDS-PAGE and blotted for TxNIP and β-actin as loading control. **B:** Collagen IV expression was analyzed by confocal microscopy and quantified by measuring pixel intensity per cell (n= 150 cells) in 3 independent experiments. Results (mean ±SE) are shown in the graphs. ***p<0.0001 vs C3H NG, **<p<0.001 vs C3H NG, and #p<0.05 vs C3H HG.

FIGURE 2. **High glucose-induced ROS and concomitant decrease in thioredoxin (Trx) activity is impaired in TxNIP-deficient Hcb-19 MC.** MCs were exposed to NG (5.6 mM) or HG (25 mM) for up to 24h. **A-C**: MC were assessed by confocal microscopy after DCF or DHE treatment for 30 min. The images were quantified as pixel intensity and expressed as % of C3H NG designated as 100 (n=3 independent experiments). **D:** H_2O_2 released by the cells was measured in 50μL cell culture media preincubated with Amplex Red reagent for 30 min (n=6; results were normalized for the number of cells). **E**: After cell lysis, Trx activity (n=5) was performed as described in Methods. Results are expressed as mean±SE. *:p<0.01 vs C3H NG, **:p<0.001 vs C3H NG , #:p<0.05 vs C3H 1h HG, ##: p<0.001 vs C3H 3h or 24h HG, and ###:p<0.0001 vs C3H 3h HG. **F:** C3H and

Hcb-19 MC were pretreated with 10μM DPI for 1h and then exposed to 1 μM and 10μM H_2O_2 for a total of 4h. The decline in ROS was assessed between 2 and 3h post-treatment (see inset for slopes) by DCF fluorescence microscopy and the relative (%) decreases in fluorescence intensities expressed as the rate of disappearance/min. Results are mean ± SE from 4 independent experiments. *:p<0.05 vs C3H at 1 μM or 10μM concentration.

FIGURE 3. High glucose (HG) effects on endogenous antioxidants in C3H and Hcb-19 (TxNIP- deficient) MC. C3H and Hcb-19 MC were cultured in NG (5.6 mM) or HG (25 mM) for 3h and 24h. Immunoblotting was performed on total cell lysates for **A**: GPx1, **B**: HO-1, **C**: MnSOD, **D**: catalase, **E**: Trx1, and **F**: Trx2 while β-actin served as loading control. The results were normalized to C3H NG, and depicted in the graphs below the respective images. Results are mean ± SE (n=4). *:p<0.05 vs C3H NG, **:p<0.001 vs C3H NG, $:p<0.05 vs C3H 3h HG, #:p<0.01 vs C3H 24h HG, and ##:p<0.001 vs C3H 3h and 24h HG

FIGURE 4. High glucose augments NADPH oxidase activity and Nox4 expression in C3H but not in Hcb-19 MC. A: NADPH oxidase activity in the total cell lysates isolated from NG (5.6 mM) or HG (25 mM) treated MC was measured as NADPH-dependent superoxide generation with the lucigenin-enhanced chemiluminescence method (n=4). **B, C**: Expression of Nox2 and Nox4 protein in total cell lysates was assessed by immunoblotting (n=4). **D, E**: *Nox2* and *Nox4* mRNA expression was assessed by real-time PCR (n=6-7). Values are mean±SE. *:p<0.01 vs C3H NG, ,#:p<0.05 vs C3H 3h HG, and ###:p<0.0001 vs C3H 3h HG.

FIGURE 5. Effect of high glucose (HG) on isoforms and subunits of NADPH oxidase in mesangial cells (MC). Growth arrested MC from C3H and Hcb-19 mice were cultured in NG (5.6 mM) or HG (25 mM) for 3h and 24h. Total cell lysates were subjected to immunoblotting for **A**: Nox1, **B**: $p47^{phox}$, **C**: $p67^{phox}$, **D**: rac1, and **E**: $p22^{phox}$, with β-actin as loading control. The results were normalized to C3H NG, and represented in graphs below the respective images. Results are mean ± SE (n=3-4 independent experiments). *:p<0.05 vs control C3H NG, #:p<0.05 vs C3H 3h HG.

FIGURE 6. Mitochondrial ROS and Nox4 protein expression in MC requires TxNIP. C3H and Hcb-19 MC were treated with NG (5.6 mM) or HG (25 mM) for the times indicated. **A:** ROS levels were determined by confocal microscopy after MitoSOX treatment for 30 min. The images were analyzed using ImageJ software and normalized to C3H NG designated as 100%**.** B: Mitochondrial and cytosolic extracts were obtained from the total cell lysates and immunoblotted for the mitochondrial markers, prohibitin, VDAC and COX IV as described in Methods. **C:** Mitochondrial expression of Nox4 and prohibitin (mitochondrial loading control) were assessed by immunoblotting. Results are mean±SE (n=3) *:p<0.05 vs control C3H NG, **:p<0.001 vs C3H NG, ##: p<0.05 vs C3H HG, and ##:p<0.001 vs C3H HG.

FIGURE 7. TxNIP knockdown in C3H MC mimics the defects in response to HG observed in Hcb-19 MC. C3H MC were transfected with 50 nM TxNIP-specific siRNA (siTxNIP) or universal negative control siRNA (scrambled, scr) for 24h and then incubated in NG (5.6 mM) or HG (25 mM) for 3h or 24h. **A, B**: Intracellular ROS and mitochondrial superoxide formation were assessed by confocal microscopy using DCF and MitoSOX respectively (n=3). **D**: Nox4 expression was measured in total cell lysates of the transfected cells by immunoblotting. Values are mean ± SE, (n=3). *:p<0.05 vs scr siRNA NG, ***:p<0.001 vs scr siRNA, #: p<0.05 vs scr HG, and ###:p<0.001 vs scr HG. **E**: Collagen IV expression was analyzed by confocal microscopy and quantified by measuring pixel intensity per cell (150 cells) in 3 independent experiments. Results mean ± SE, (n=3) are depicted in the graphs.

FIGURE 8. Overexpression of TxNIP in Hcb-19 MC restores mitochondrial ROS and Nox4 expression. Hcb-19 cells were transduced with

GFP (AdGFP) or TxNIP (AdTxNIP) adenoviruses and C3H cells with AdGFP alone to serve as a control. After 24h, cells were growth arrested for 48h and then exposed to NG (5.6 mM) or HG (25 mM) for 3h. **A**: Mitochondrial superoxide production in the MC was determined with MitoSOX dye by confocal microscopy. Quantification is illustrated in the graph. Results are mean±SE. *:$p<0.05$, and **:$p<0.001$ vs AdGFP C3H NG. **B**: Immunoblotting for Nox4 and TxNIP was performed using lysates from Hcb19 MC transduced with varying concentrations of AdTXNIP (25×10^7, 5×10^8 and 1×10^9 ifu/ml) in NG or HG. Results are mean ± SE (n=4). *:$p<0.05$ vs AdGFP Hcb19 NG.

FIGURE 9. TxNIP-deficient Hcb-19 MC show impaired mitochondrial glucose metabolism and increased lactate production. Growth arrested MC (C3H, Hcb-19) were exposed to NG (5.6mM) or HG (25mM) for up to 24h. **A**: Lactate concentrations in the cell culture media. Results are mean ± SE (n=4 *:$p<0.05$ vs C3H NG, and #:$p<0.05$ vs Hcb-19 HG. **B**: MC fluorescence was observed by confocal microscopy after JC-1 treatment for 30 min. The images were analyzed using Image J software and normalized to C3H NG. Quantification is illustrated in the graph. Results are mean ± SE (n=3). **:$p<0.001$ vs C3H NG, and ##:$p<0.001$ vs C3H 3h and 24h HG.

Fig 1

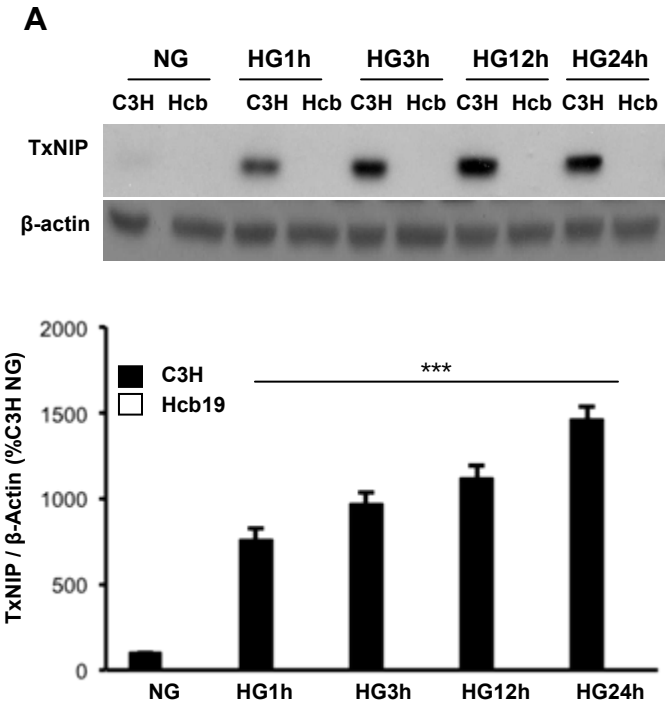
A
NG
HG1h
HG3h
HG12h
HG24h
C3H Hcb C3H Hcb C3H Hcb C3H Hcb C3H Hcb
TxNIP
β-actin
TxNIP / β-Actin (%C3H NG)
2000
1500
1000
500
0
C3H
Hcb19
***
NG
HG1h
HG3h
HG12h
HG24h

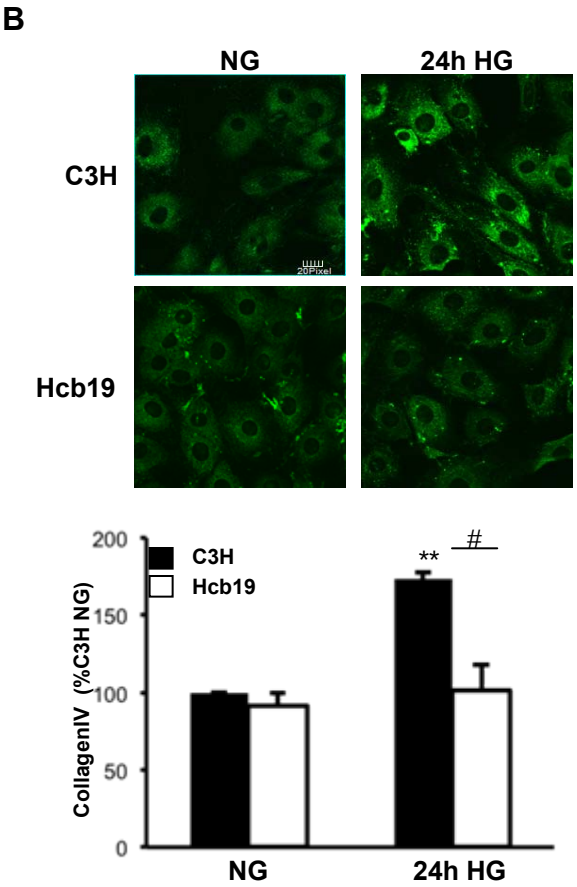
B
NG
24h HG
C3H
Hcb19
CollagenIV (%C3H NG)
200
150
100
50
0
C3H
Hcb19
**
#
NG
24h HG

Fig 2

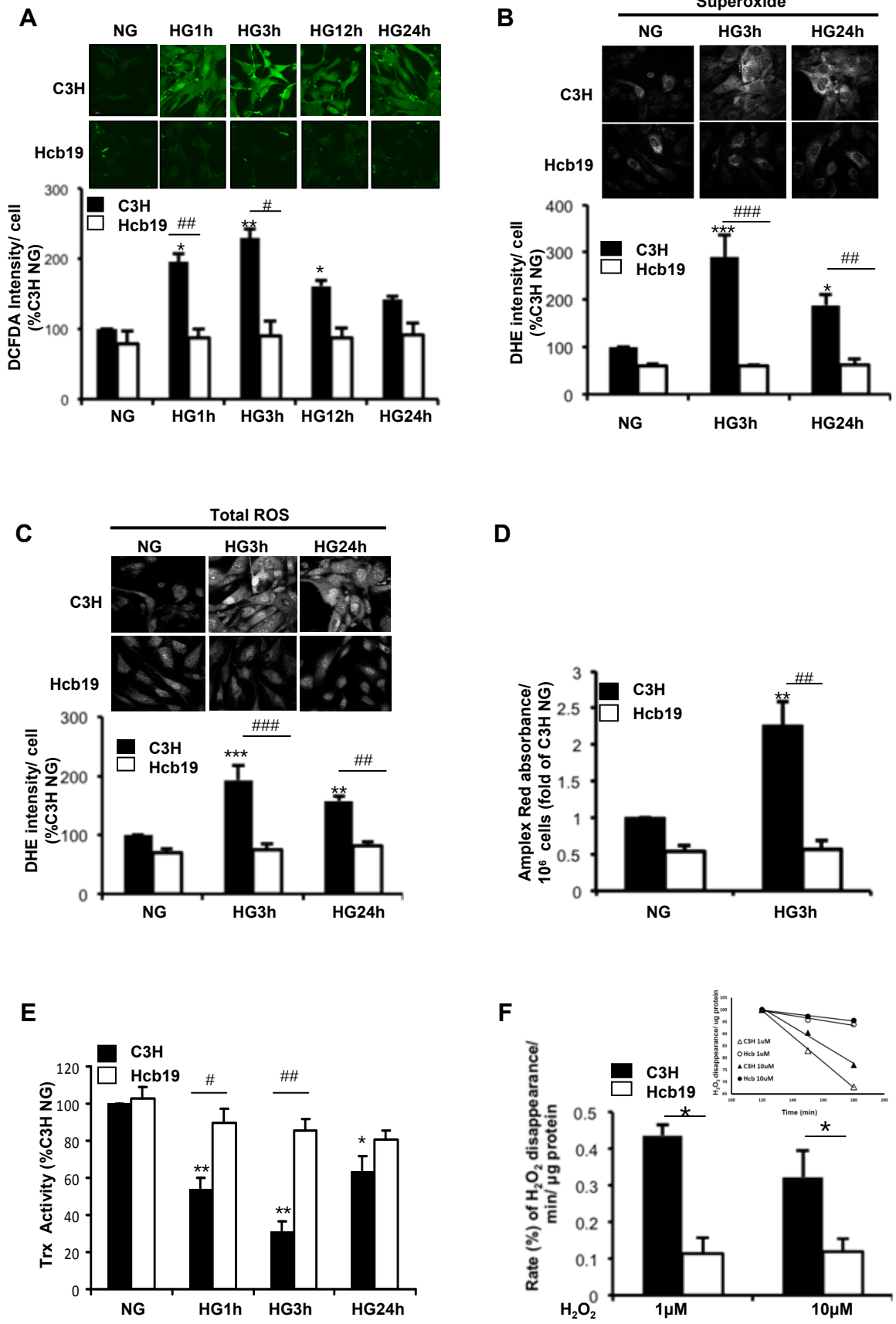
A
NG
HG1h
HG3h
HG12h
HG24h
C3H
Hcb19
DCFDA Intensity/ cell (%C3H NG)
B
Superoxide
DHE intensity/ cell (%C3H NG)
C
Total ROS
D
Amplex Red absorbance/ 10⁶ cells (fold of C3H NG)
E
Trx Activity (%C3H NG)
F
Rate (%) of H2O2 disappearance/ min/ µg protein
H2O2
1µM
10µM
Time (min)
C3H 1uM
Hcb 1uM
C3H 10uM
Hcb 10uM

Fig 3

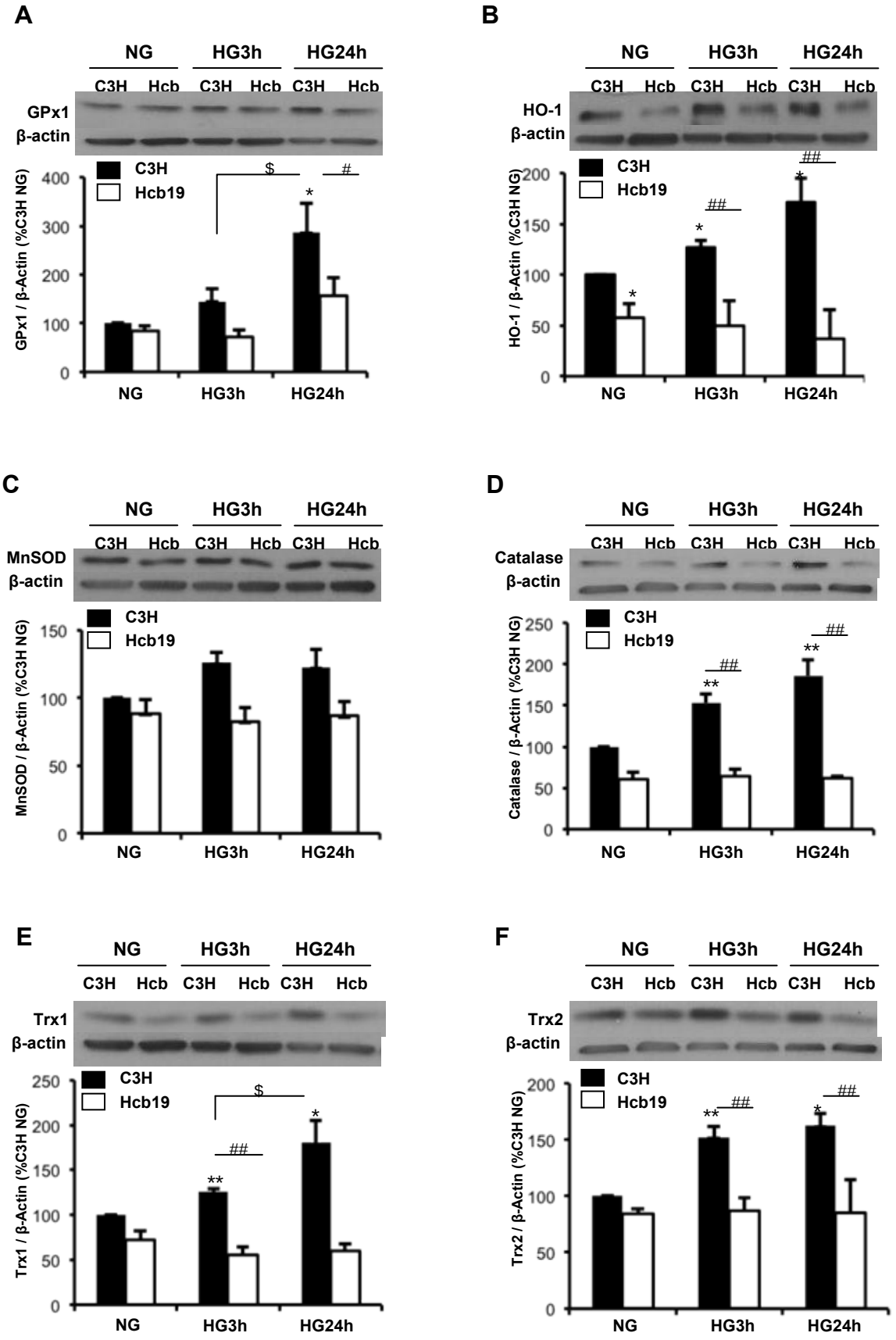
A
NG
HG3h
HG24h
C3H
Hcb
GPx1
β-actin
C3H
Hcb19
GPx1 / β-Actin (%C3H NG)
B
HO-1
β-actin
HO-1 / β-Actin (%C3H NG)
C
MnSOD
β-actin
MnSOD / β-Actin (%C3H NG)
D
Catalase
β-actin
Catalase / β-Actin (%C3H NG)
E
Trx1
β-actin
Trx1 / β-Actin (%C3H NG)
F
Trx2
β-actin
Trx2 / β-Actin (%C3H NG)

Fig 4

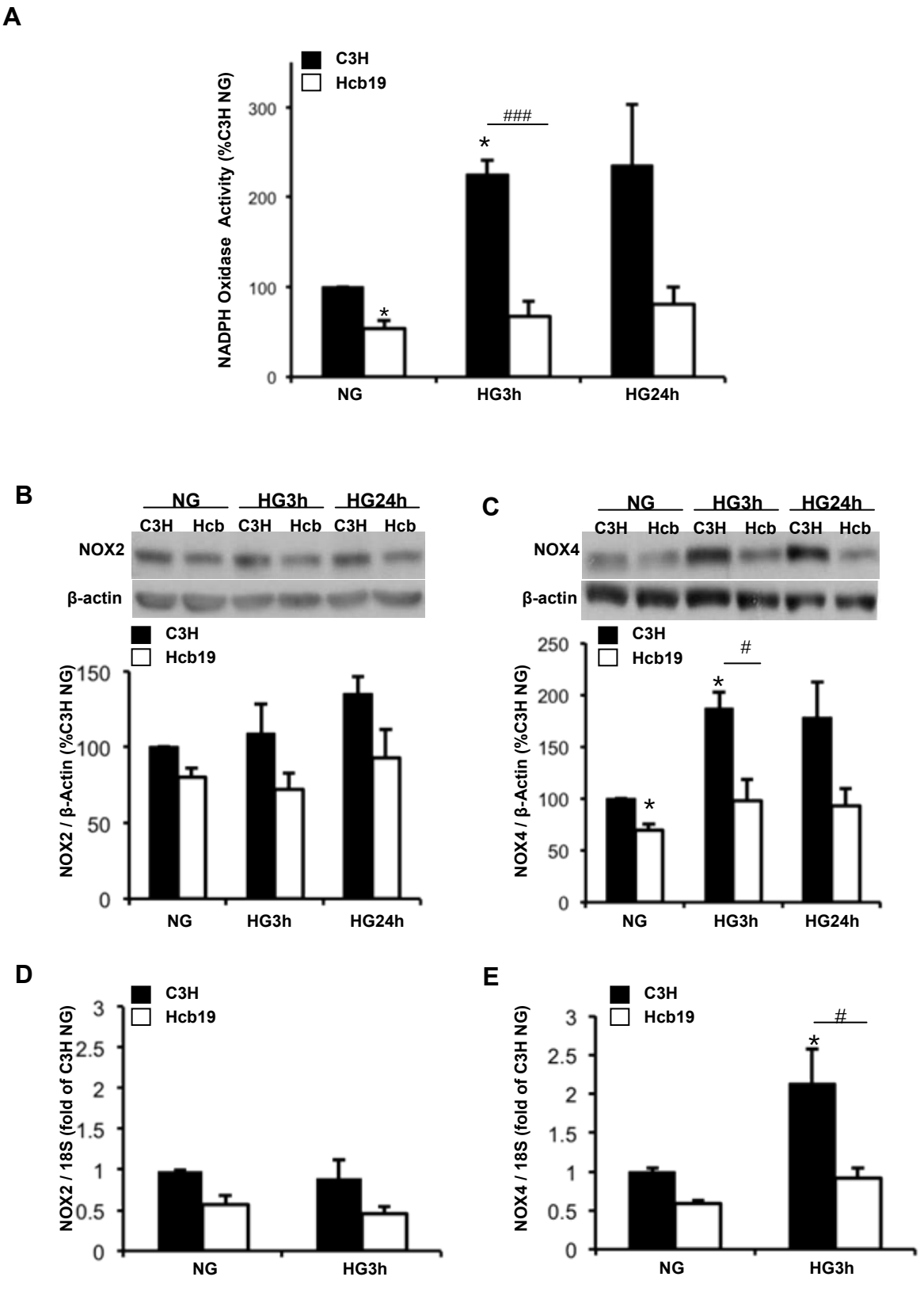
A
C3H
Hcb19
NADPH Oxidase Activity (%C3H NG)
300
200
100
0
###
*
*
NG
HG3h
HG24h
B
NG
HG3h
HG24h
C3H
Hcb
C3H
Hcb
C3H
Hcb
NOX2
β-actin
C3H
Hcb19
NOX2 / β-Actin (%C3H NG)
150
100
50
0
NG
HG3h
HG24h
C
NG
HG3h
HG24h
C3H
Hcb
C3H
Hcb
C3H
Hcb
NOX4
β-actin
C3H
Hcb19
#
*
*
NOX4 / β-Actin (%C3H NG)
250
200
150
100
50
0
NG
HG3h
HG24h
D
C3H
Hcb19
NOX2 / 18S (fold of C3H NG)
3
2.5
2
1.5
1
0.5
0
NG
HG3h
E
C3H
Hcb19
#
*
NOX4 / 18S (fold of C3H NG)
3
2.5
2
1.5
1
0.5
0
NG
HG3h

Fig 5

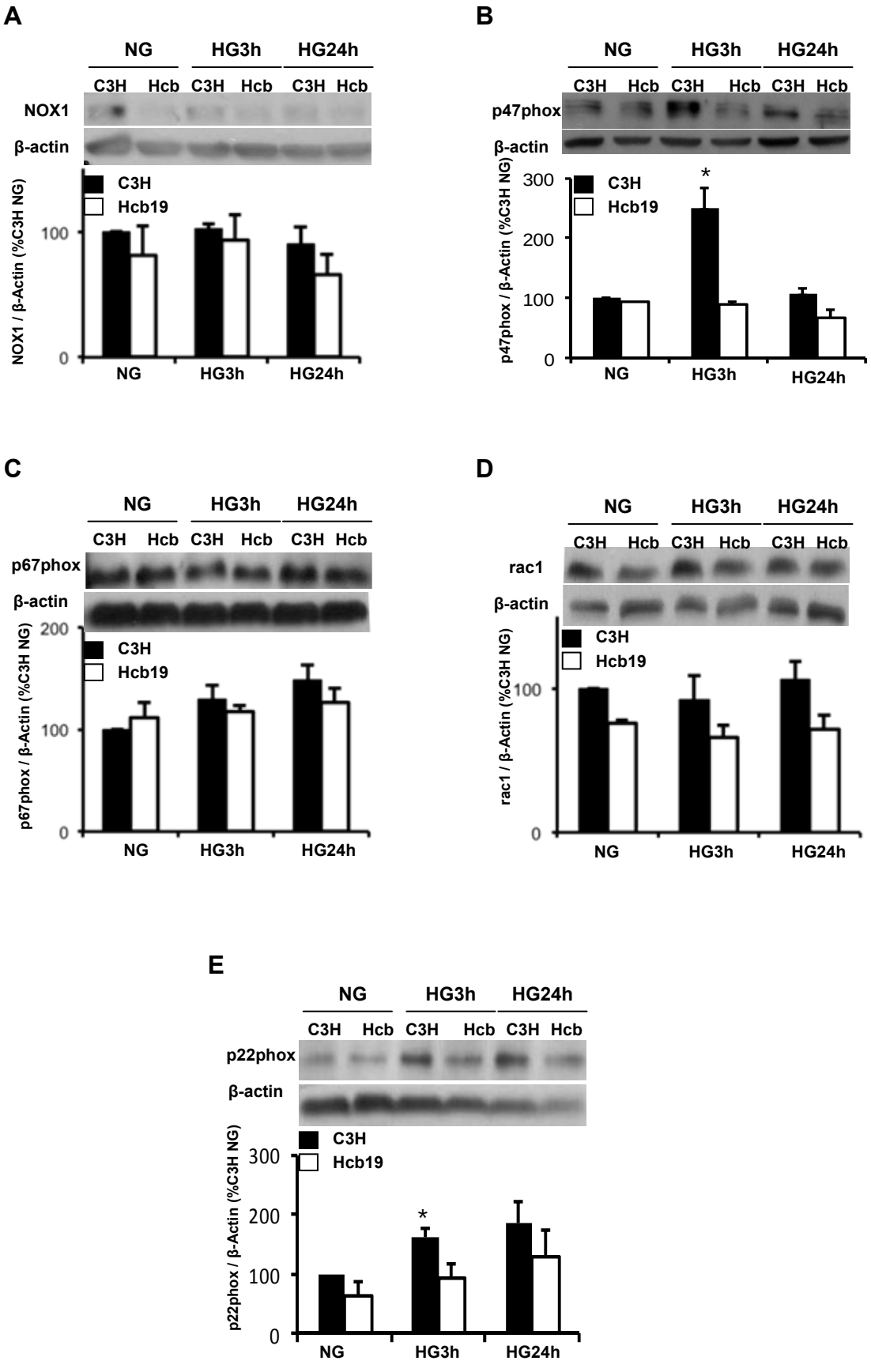
A
NG
HG3h
HG24h
C3H
Hcb
NOX1
β-actin
C3H
Hcb19
NOX1 / β-Actin (%C3H NG)
100
0
NG
HG3h
HG24h
B
p47phox
β-actin
300
200
100
0
*
p47phox / β-Actin (%C3H NG)
C
p67phox
β-actin
200
p67phox / β-Actin (%C3H NG)
D
rac1
β-actin
rac1 / β-Actin (%C3H NG)
E
p22phox
β-actin
p22phox / β-Actin (%C3H NG)

Fig 6

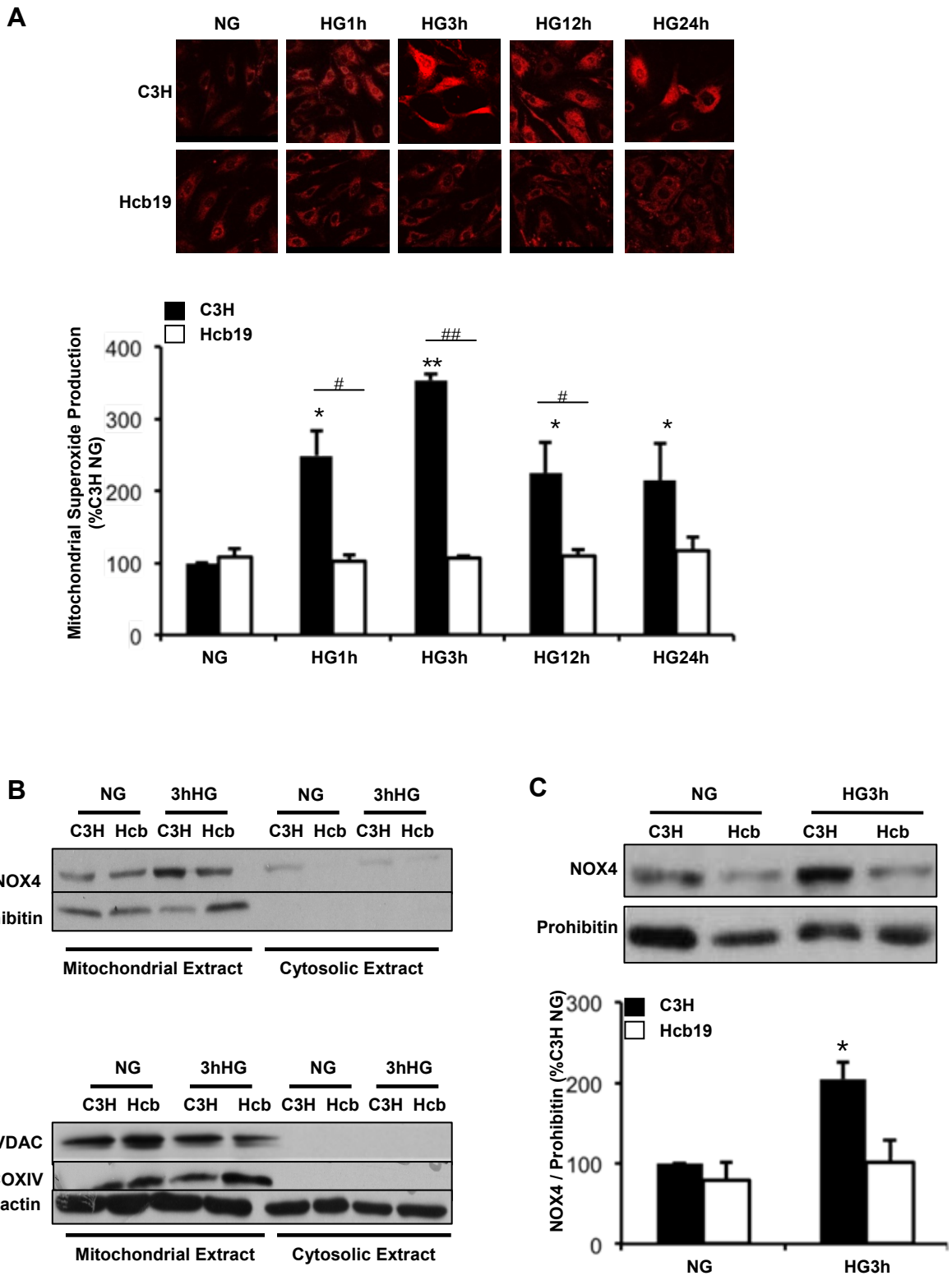
A
NG
HG1h
HG3h
HG12h
HG24h
C3H
Hcb19
C3H
Hcb19
Mitochondrial Superoxide Production (%C3H NG)
400
300
200
100
0
#
##
*
**
*
*
NG
HG1h
HG3h
HG12h
HG24h
B
NG
3hHG
NG
3hHG
C3H Hcb C3H Hcb C3H Hcb C3H Hcb
NOX4
Prohibitin
Mitochondrial Extract
Cytosolic Extract
NG
3hHG
NG
3hHG
C3H Hcb C3H Hcb C3H Hcb C3H Hcb
VDAC
COXIV
β-actin
Mitochondrial Extract
Cytosolic Extract
C
NG
HG3h
C3H Hcb C3H Hcb
NOX4
Prohibitin
NOX4 / Prohibitin (%C3H NG)
300
200
100
0
C3H
Hcb19
*
NG
HG3h

Fig 7

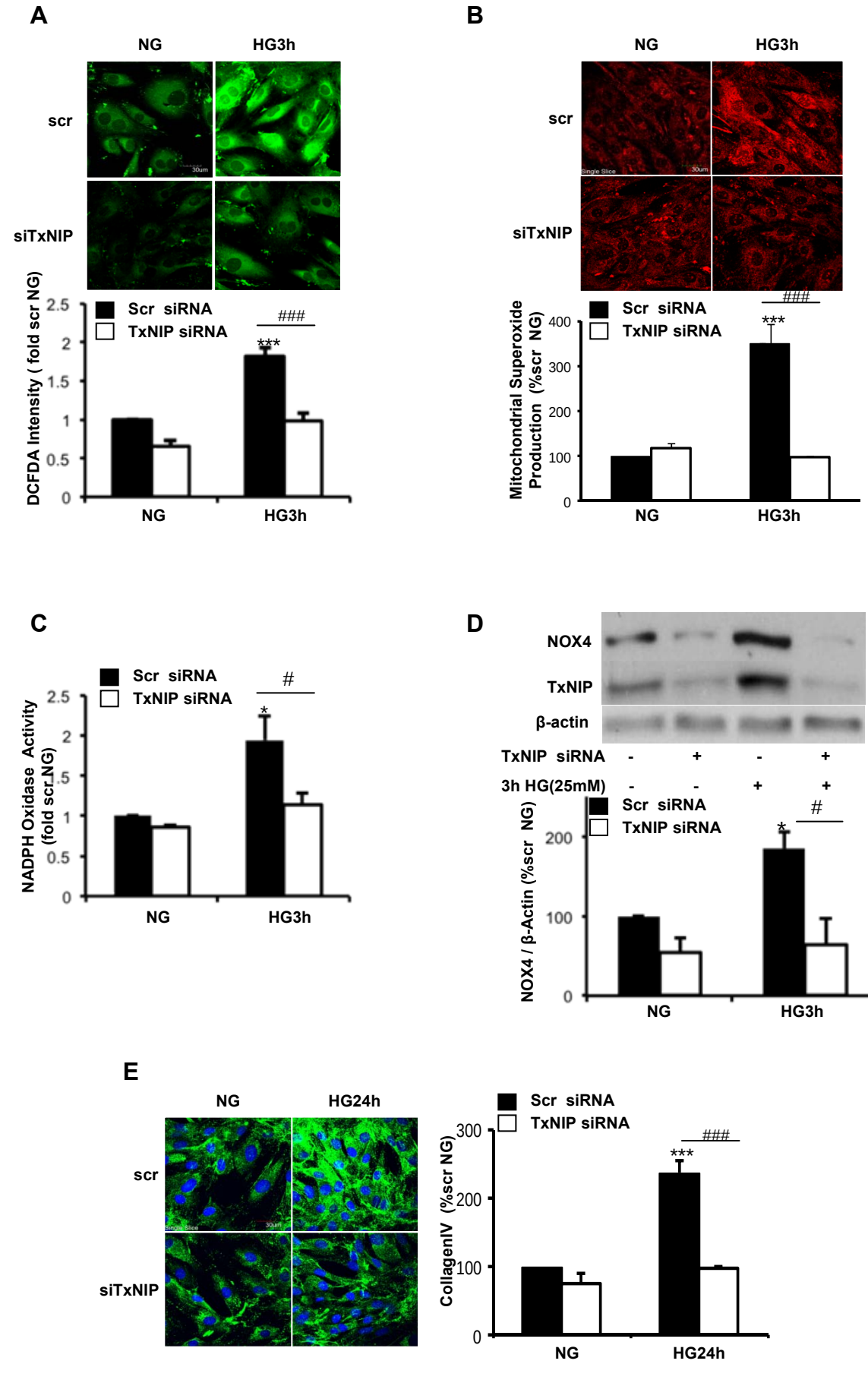
A
NG
HG3h
scr
siTxNIP
DCFDA Intensity (fold scr NG)
Scr siRNA
TxNIP siRNA
###
***
B
Mitochondrial Superoxide Production (%scr NG)
C
NADPH Oxidase Activity (fold scr NG)
#
*
D
NOX4
TxNIP
β-actin
TxNIP siRNA
3h HG(25mM)
NOX4 / β-Actin (%scr NG)
E
HG24h
CollagenIV (%scr NG)

Fig 8

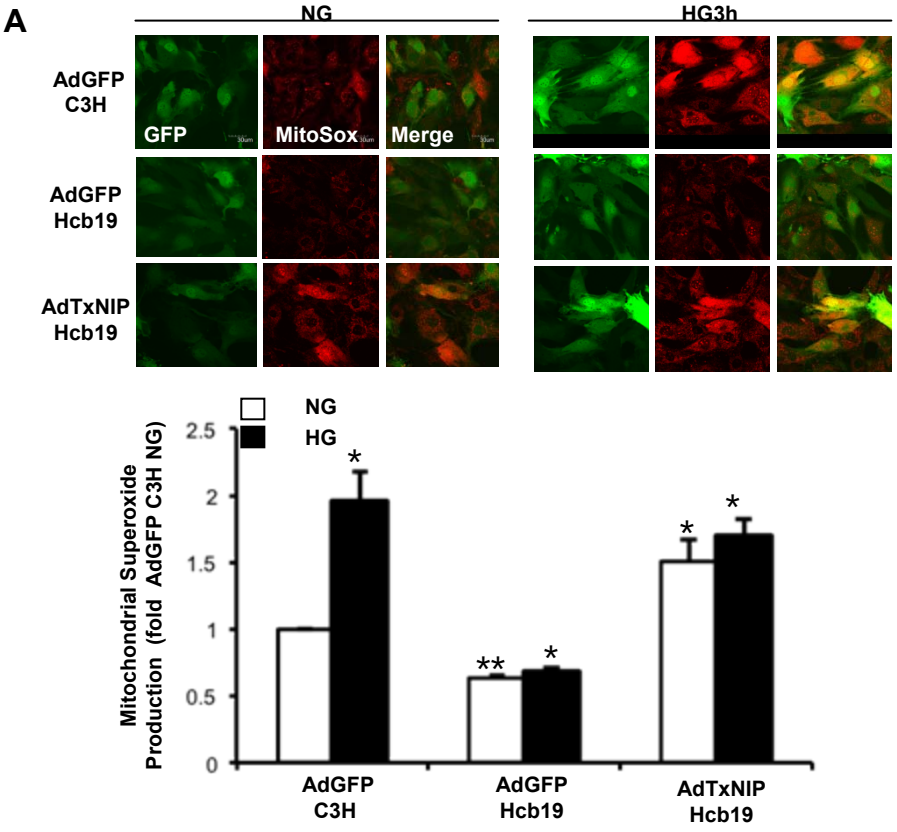
A
NG
HG3h
AdGFP C3H
AdGFP Hcb19
AdTxNIP Hcb19
GFP
MitoSox
Merge
NG
HG
Mitochondrial Superoxide Production (fold AdGFP C3H NG)
2.5
2
1.5
1
0.5
0
*
**
*
*
*
AdGFP C3H
AdGFP Hcb19
AdTxNIP Hcb19

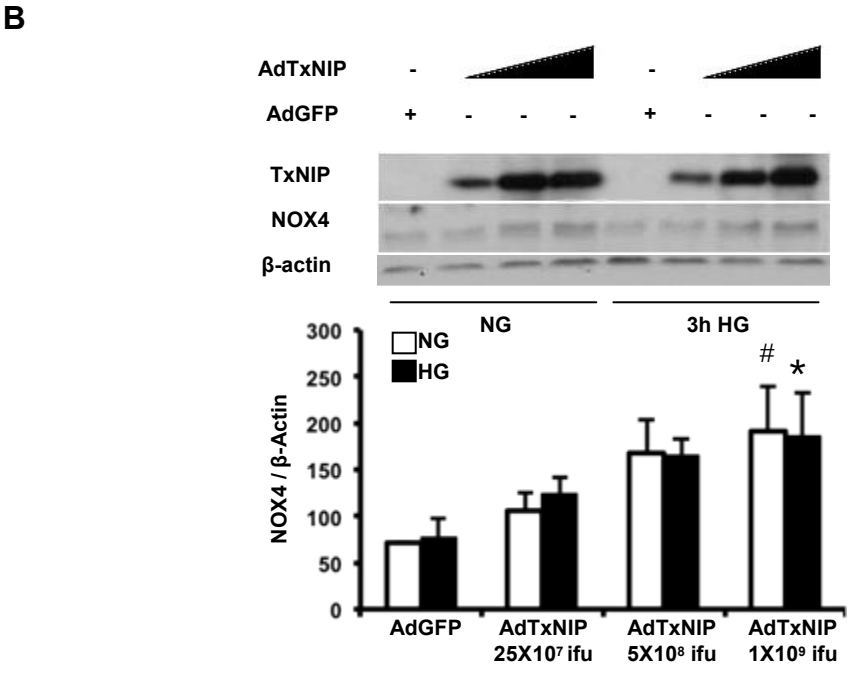
B
AdTxNIP
AdGFP
-
+
TxNIP
NOX4
β-actin
NG
3h HG
NG
HG
NOX4 / β-Actin
300
250
200
150
100
50
0
#
*
AdGFP
AdTxNIP 25X10⁷ ifu
AdTxNIP 5X10⁸ ifu
AdTxNIP 1X10⁹ ifu

Fig 9

A

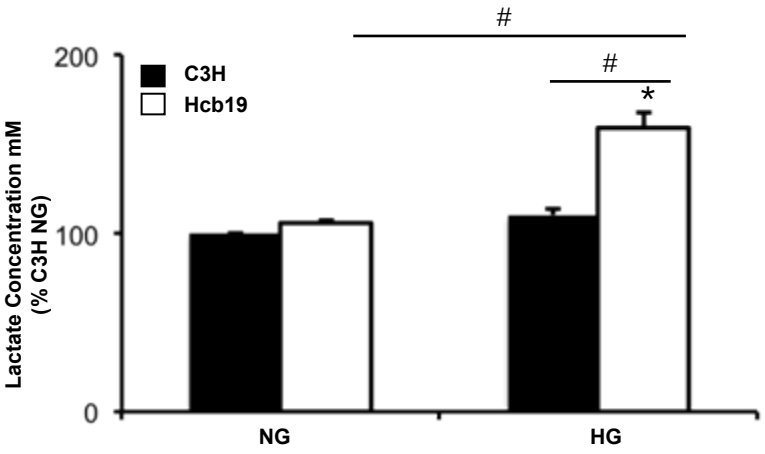
#
#
*
C3H
Hcb19
200
100
0
Lactate Concentration mM
(% C3H NG)
NG
HG

B

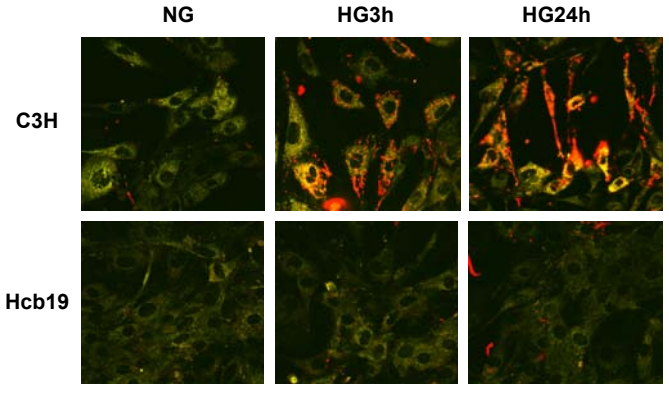
NG
HG3h
HG24h
C3H
Hcb19

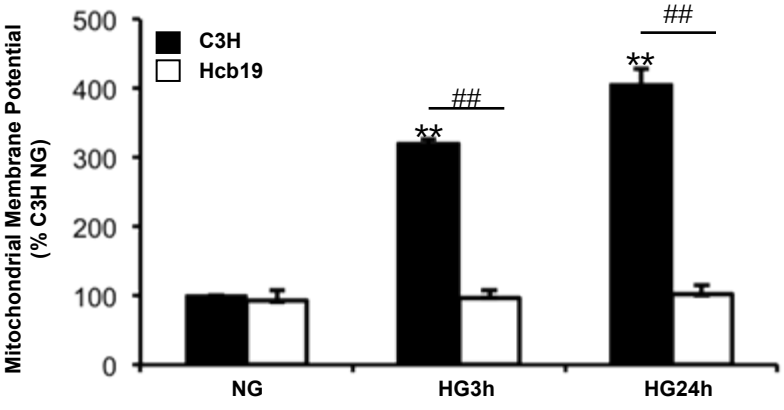
##
##
**
**
C3H
Hcb19
500
400
300
200
100
0
Mitochondrial Membrane Potential
(% C3H NG)
NG
HG3h
HG24h

Thioredoxin-interacting protein mediates high glucose-induced reactive oxygen species (ROS) generation by mitochondria and the NADPH oxidase, Nox4, in mesangial cells

Anu Shah, Ling Xia, Howard Goldberg, Ken W. Lee, Susan E. Quaggin and Ivan G. Fantus

J. Biol. Chem. published online January 17, 2013
